Research Article Vol. 32, No. 5 / 26 Feb 2024 / Optics Express 7473
Optics EXPRESS

WaveGate: a versatile tool for temporal shaping of synchrotron beams

D. Schmidt,[1] D. Hensel,[2] M. V. Petev,[1] M. Khosla,[2] M. Brede,[2] S. Vadilonga,[3] and P. Gaal[1,2,*]

[1]TXproducts UG (haftungsbeschränkt), Luruper Hauptstr. 1, 22547 Hamburg, Germany
[2]Leibniz-Institut für Kristallzüchtung, Max-Born-Str. 2, 12489 Berlin, Germany
[3]Helmholtz-Zentrum für Materialien und Energie, Albert-Einstein-Str. 15, 12489 Berlin, Germany
*peter.gaal@ikz-berlin.de

Abstract: We present a full performance characterization of a solid state pulse picker for hard x-ray pulses at synchrotrons. The device is called WaveGate. Specifically, we quantify its efficiency (>30 %), timing capabilities (switching times between 100 ns and ms), on-off contrast (>10^4) and influence on the coherence properties of the incident x-ray beam. In addition, we discuss the implementation of the WaveGate in an optical pump - x-ray probe setup. Even if single pulse selection is performed by external detector gating, the WaveGate drastically increases the efficiency of a measurement. Finally, we introduce advanced timing schemes that can be realized by modulating the time structure of the synchrotron beam.

© 2024 Optica Publishing Group under the terms of the Optica Open Access Publishing Agreement

1. Introduction

Users of synchrotron radiation have become accustomed to a certain temporal pulse structure emitted by the storage ring. Typical parameters are temporal gaps between x-ray pulses of 10 ns - 1000 ns [1–4] and an x-ray pulse duration of approximately 100 ps [5,6]. Due to the architecture of a synchrotron, any time structure set by the machine affects all beamlines and experimental stations connected to the storage ring. A given time structure sets limitations on the feasibility of an experiment. To mitigate these constraints and address the divers and sometimes conflicting requirements of different user communities, almost all synchrotron facilities provide changing operation modes. This adds additional planning and organization effort while many user requests still cannot be completely fulfilled. A real solution overcoming the constraints imposed by the synchrotron operation mode consists in tailoring the time structure of the synchrotron radiation at the level of the beamline using optical elements. Such optics enable beam conditioning specifically for each experiment, similar to e.g. selecting the beams energy with a monochromator. In this article, we introduce so-called Active X-Ray Optics (AXOs) for exactly that purpose.

The capabilities of AXOs are schematically shown in Fig. 1. Panel a) depicts a typical pulse train emitted from a synchrotron storage ring with the characteristic parameters *pulse separation* and *pulse duration*. Panel 1(b) illustrates the operation of two different AXOs, namely the WaveGate pulse picker and the PicoSwitch [7,8]. The former is used to block impinging x-ray pulses over a highly flexible temporal range. The latter acts as switchable mirror to slice the central part of the x-ray pulse, thus reducing the duration and increasing the temporal resolution accordingly. In this article we solely focus on the capabilities of the WaveGate pulse picker. The working principle of our device is described in detail elsewhere [9]. Here, we specify and demonstrate the main performance parameters of the device, such as the gating times, the efficiency of transmitted pulses and the on-off contrast. We also characterize the impact on the x-ray beam coherence and provide first examples for user cases, e.g., the generation of arbitrary pulse sequences which can be used for advanced timing schemes [10]. An example of such an arbitrary pulse sequence is shown in Fig. 1(c).

#515884 https://doi.org/10.1364/OE.515884
Journal © 2024 Received 13 Dec 2023; revised 3 Jan 2024; accepted 8 Jan 2024; published 15 Feb 2024

Optics EXPRESS

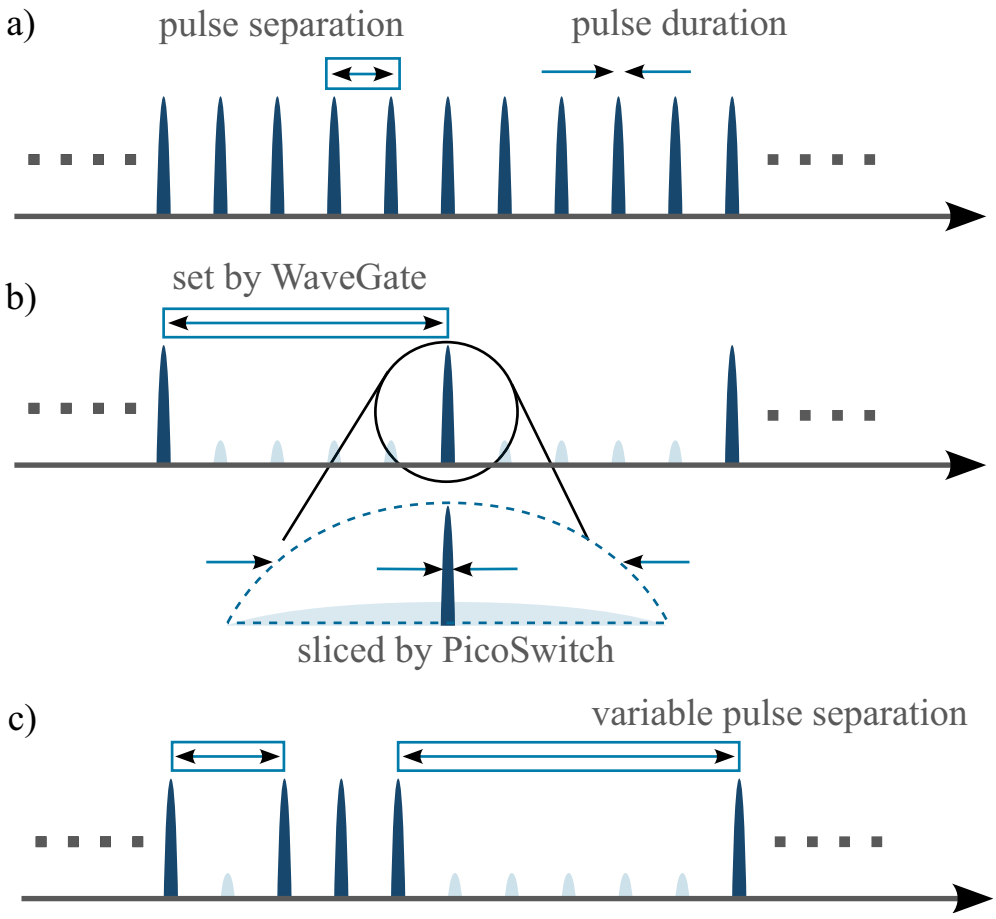

Fig. 1. Time structure of synchrotron beams: a) Time structure of the synchrotron pulse train determined by pulse duration and pulse separation. b) Reduction of the x-ray pulse repetition rate by picking every 5th pulse with the WaveGate. The suppressed pulses are shown in light blue. The zoom on the transmitted pulse in the center depicts pulse shortening by the PicoSwitch [8]. c). Generation of a variable pulse pattern for advanced timing schemes. Similar measured pulse pattern are depicted in Fig. 6.

Optics EXPRESS

2. WaveGate pulse picker characterization

Figure 2(a) depicts a schematic of the WaveGate pulse picker. The setup consists of two crystals from the same piezoelectric substrate, referred to as active and analyzer crystal, respectively. The crystals are mounted in a double crystal monochromator (DCM) geometry. We fabricate interdigitated transducers (IDTs) on the surface of the active, piezoelectric crystal to convert a high-frequency electric field into a surface acoustic wave (SAW). The RF signal is generated by the WaveGate signal generator connected to the IDT.

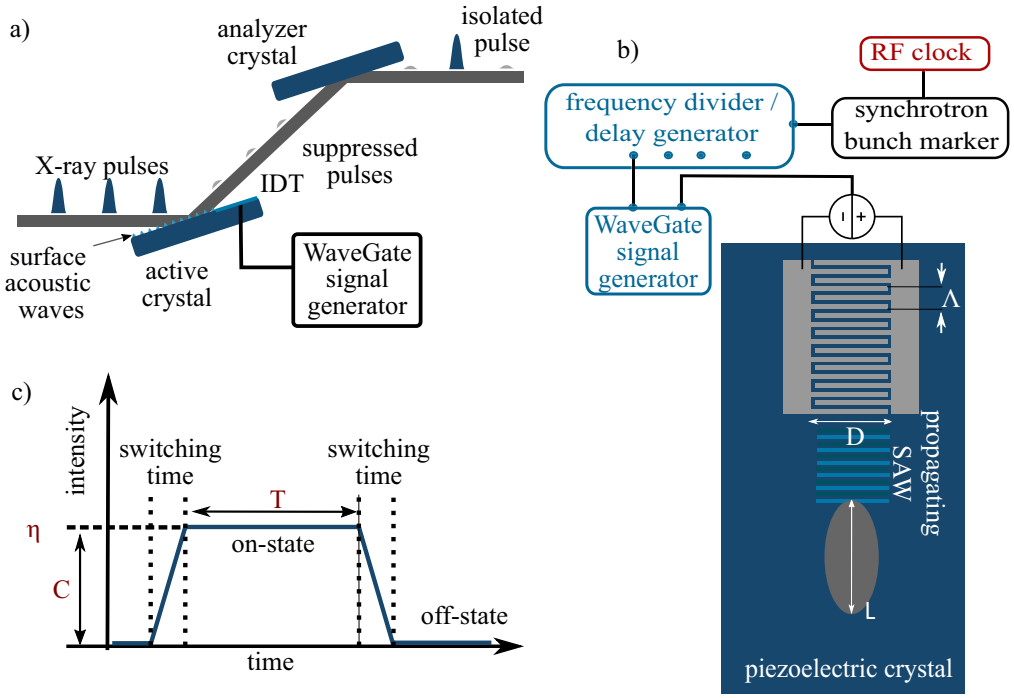

Fig. 2. WaveGate gating tool: a) Sketch of the WaveGate pulse picker setup. The active and analyzer crystal are mounted in a double crystal monochromator (DCM) geometry. Transmission and suppression of incident pules is controlled by the WaveGate signal generator. Its RF output is fed to the interdigital transducer (IDT) on the active crystal. b) Sketch of the active crystal and necessary electronics for synchronization to a synchrotron bunch marker and for the generation of surface acoustic waves (SAWs) in the piezoelectric substrate. The IDT is shown in light gray with a period Λ and an aperture size D. The SAW propagates along the crystal surface through the footprint of an impinging x-ray pulse (dark gray) with length L. c) Grafical representation of the performance parameters efficiency (η), contrast (C), gate opening time (T) and switching time.

A propagating SAW alters the diffraction condition

$$\vec{G} + \vec{q}_{\mathrm{SAW}} = \vec{k}_{out} - \vec{k}_{in}, \tag{1}$$

where $\vec{G}$ is the reciprocal lattice vector of the substrate and $\vec{k}_{out}$, $\vec{k}_{in}$ are the wavevectors of the incident and diffracted x-ray beam, respectively. By tuning the incidence angle of the x-ray beam accordingly, x-ray pulses impinging on the active crystal are either diffracted towards the analyzer crystal or penetrate into the active crystal along their original trajectory, depending on the deformation of the substrate induced by propagating SAWs. The analyzer crystal diffracts all

Optics EXPRESS

incident pulses following $\vec{G} = \vec{k}_{out} - \vec{k}_{in}$. Thus, transmission of x-ray pulses can be controlled with the external RF signal.

A closer view on the active crystal is shown in Fig. 2(b). The IDT structure is shown in gray on the surface of the piezoelectric substrate which is depicted in blue. The IDT spatial period Λ determines the wavevector $q_{SAW} = 2\pi/\Lambda$ of the generated SAW. The SAW frequency $f_{SAW} = \frac{v_{SAW}}{\Lambda}$ for a given q_{SAW} depends on the wave velocity v_{SAW} in the substrate. A signal generator delivers high-frequency (RF) voltage bursts to generate SAWs at the eigenfrequency of the IDT. It is synchronized to the x-ray pulses emitted by the storage ring via the synchrotron bunch marker. An additional frequency divider / delay generator unit allows to select the repetition rate as well as the opening time and the delay of the temporal gate.

Figure 3(b) also depicts the footprint of an incident x-ray pulse shaded in dark gray with an extension L in direction of the SAW propagation. As soon as the SAW has propagated through the whole length of the footprint, the beam can be fully diffracted [c.f. Eq. (1)]. We call this propagation time $t_{on/off} = L/v_{SAW}$ the *switching time*. The WaveGate remains in the *on-state* as long as the SAW fully overlaps with the x-ray footprint on the active crystal. The duration of the *on-state* directly follows the duration of the RF burst set by the delay generator.

The temporal gate is sketched in Fig. 2(c) with the main performance parameters highlighted in dark red. These parameters are the *temporal gate width* T, the diffraction efficiency in the *on-state* η and the *on-off contrast* C. The latter quantity is the ratio of integrated photon counts while the WaveGate is turned on and off. Measurement of the contrast requires gating of the x-ray detector as discussed in section 3.

A measurement of these quantities is depicted in Fig. 2(a)-(c). We employed lithium niobate ($LiNbO_3$) as piezoelectric substrate for the active and analyzer crystal, respectively. The crystals were oriented in the rotated Y-cut or 128° Y-X configuration. The crystal surface is parallel to the (104) lattice plane and the IDT wavevector points along the x-direction of the crystal with a SAW velocity $v_{SAW} = 3.5\ \frac{nm}{ps}$. The IDT excites so-called acoustic Rayleigh modes [11] with a period of Λ=4 μm. The acoustic deformation extends about $\Lambda/2$ into the substrate, i.e., two times the extinction length of the incident x-ray pulse [12]. Measurements were performed at the XPP instrumental station of the KMC3 beamline at the BESSY II synchrotron source [13] and at the situ x-ray diffraction beamline P23 at the Petra III synchrotron at DESY. At KMC3 we set the energy of the monochromatic ($\Delta E/E_0 = 10^{-3}$) x-ray beam to 8 keV. At P23 we choose a photon energy of 14.4 keV at a relative bandwidth $\Delta E/E_0 = 10^{-4}$.

First we discuss measurements of temporal gates with opening times from 100 ns to 100 µs depicted in Fig. 3(a). Note the logarithmic time axis in the figure to accommodate the timescales of the temporal gates which differ by orders of magnitude. The x-ray beam size was set to 50 µm and the Bragg angle of the (104) plane of the active crystal was 14.578 °. This results in an x-ray beam footprint of L = 200 µm and in a minimal switching time $t_{on/off}$ = 57 ns. The shortest gate of 100 ns duration shown in Fig. 3(a) is about the fastest gate that can be realized in this configuration. Note that our device can produce even faster gates with opening times of less than 10 ns at the cost of a reduced switching contrast [14]. The flexibility of the WaveGate is demonstrated by gating times of 1 µs, 10 µs and 100 µs (from dark to light blue), respectively. We like to point out that any gate opening time can be selected by simply changing the duration of the RF burst without additional alignment of the WaveGate. Once the WaveGate is integrated in a setup, the gate opening time can be selected by entering a single command in the software control.

Second we discuss the efficiency of the WaveGate pulse picker in the *on-state*. Figure 3(b) depicts a rocking scan of the active crystal in the *on-* and *off-state* (dark and light blue curve, respectively). The measurements were performed in the standard DCM configuration shown in Fig. 2(a). For easy evaluation we normalized the diffracted intensity to the intensity incident on the active crystal. The propagating SAW generates side bands of the (104) reflex as derived in

Optics EXPRESS

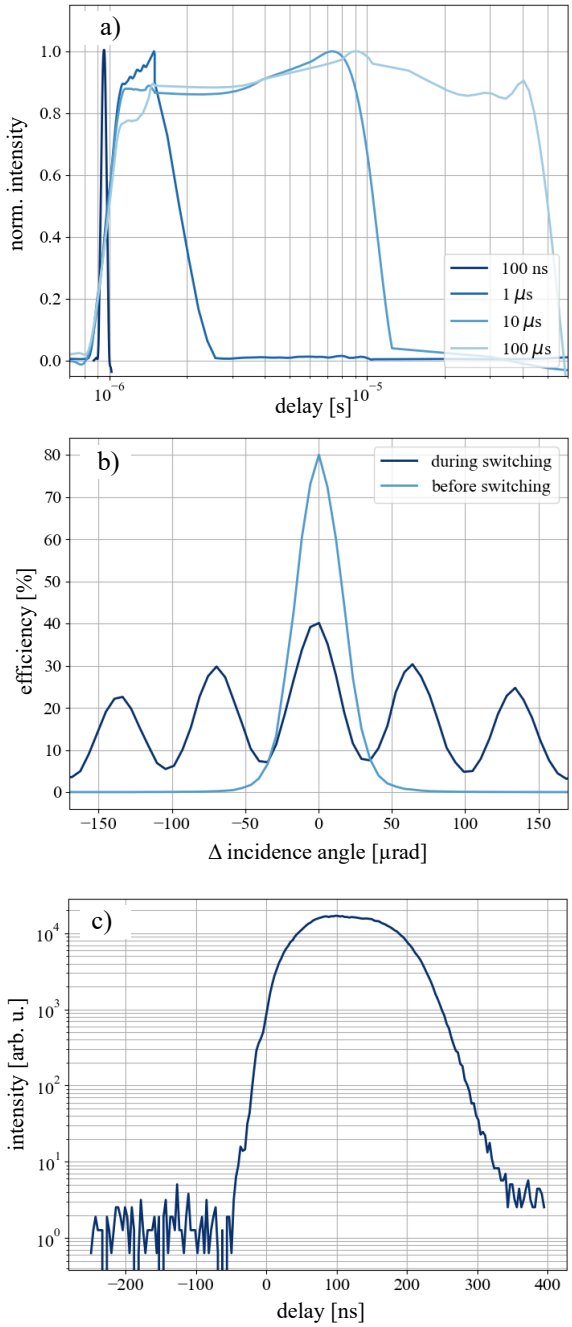

Fig. 3. Measurement of key performance parameters: a) Temporal gates with a duration of 100 ns, 1 μs, 10 μs and 100 μs (from dark to light blue), respectively. Note the logarithmic timescale to accommodate the large variation of gating times. b) Diffraction efficiency in %, i.e. normalized to the intensity incident on the WaveGate. c) Measurement of the on-off contrast of 10^4. The result may be biased by the limited dynamic range of the measurement.

Optics EXPRESS

Equ. (1). They appear in the dark blue curve in Fig. 3(b) and reach a diffraction efficiency of 30% of the incident beam.

Third we discuss the on-off contrast of the WaveGate pulse picker, which is shown in Fig. 3(c). The measurement is similar to the gate scans shown in Fig. 3(a), however, we use a longer integration time to accumulate better statistics, especially in the off-state. We measure an on-off contrast of better than 10^4, however, the measurement is still limited by photon statistics.

To conclude the device characterization, we now discuss how the WaveGate active crystal influences the coherence properties of an impinging x-ray beam. To determine the lateral coherence length we introduce an aperture with variable opening size in the diffracted beam. For opening sizes within the lateral coherence length, we observe diffraction satellites due to coherent scattering at the apertures boundaries. Figure 4(a) sketches the experimental setup which was implemented at the ID01 beamline at the European Synchrotron ESRF. The x-ray beam had a photon energy of 9 keV and an area of 100 µm × 100 µm. As a variable aperture we used a pair of vertical and horizontal slits which we mounted on the detector arm 0.3 m away from the rotation center. Images of the coherent beam were recorded with a high resolution CMOS detector (Andor Zyla) with pixel size of 7 µm × 7 µm at a distance of 6.5 m from the rotation center.

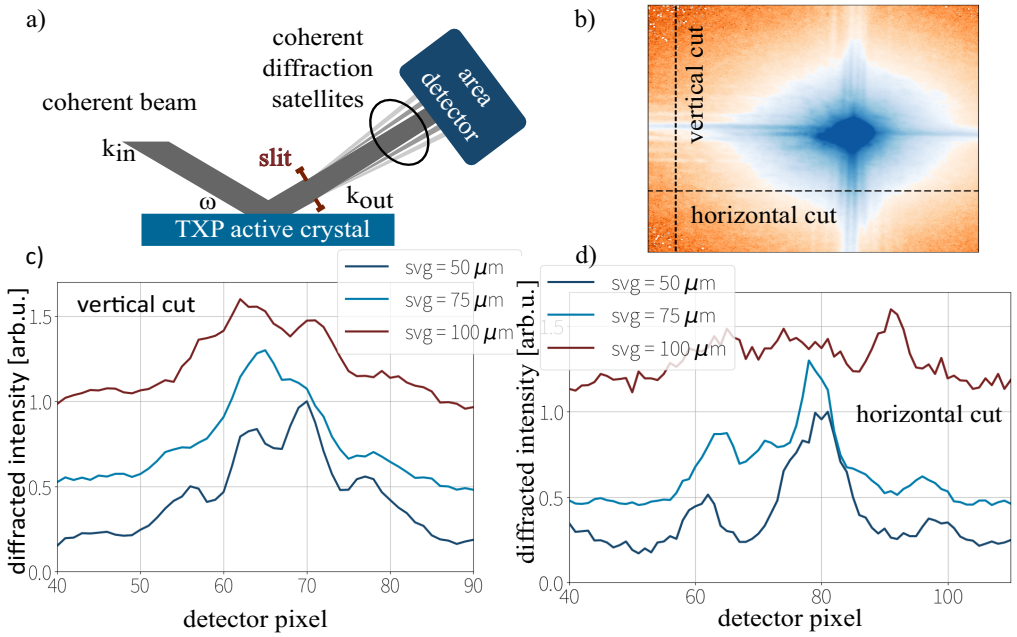

Fig. 4. Impact of the WaveGate on the beam coherence: a) Experimental setup to determine the lateral coherence of the diffracted beam after the active crystal of the WaveGate. A pair of variable slits is used as aperture to generate coherent diffraction satellites on the detector. b) detector image recorded at an opening of 50 μm. The vertical and horizontal dashed lines indicate the positions of the line cuts shown below. c) and d) intensity plots along the line cuts indicated in b) at aperture openings of 50 μm, 75 μm and 100 μm, respectively.

Figure 4(b) depicts a typical detector image. The aperture size was 50 μm. Figure 4(c) and (d) show diffracted intensity on a vertical and horizontal cut, indicated by the dashed lines in Fig. 4(b), for 50 μm (dark blue), 75 μm (light blue) and 100 μm (red) aperture sizes. Modulations of the diffracted intensity appear for all measurements with an aperture size smaller than the beam size. These coherent diffraction features become stronger if the aperture size is reduced. Note that due to the large slit opening, the observed features do not constitute a simple slit diffraction

Optics EXPRESS

pattern but rather a complicated superposition of diffraction at the slit and limited resolution of the detector. Due to the limited beamtime available we could not repeat these measurements in the direct beam to quantify absolute changes of the coherence properties. However, our observation of coherent scattering features in the diffracted beam even at large aperture sizes indicate that the WaveGate active crystal does not noticeably deteriorate the coherence properties of an x-ray beam.

3. WaveGate pulse picker application examples

In this section we employ the WaveGate pulse picker in real experimental setups and present a few application examples. The first measurement example was performed at the Petra III beamline P23. Our experimental setup is shown in Fig. 5(a). The synchrotron operated in 40 bunch mode with a temporal x-ray pulse spacing of 192 ns. We installed the WaveGate setup in the experimental hutch approximately 2 m upstream of the sample position in the slightly focused x-ray beam.

For time-dependent studies we employ a pulsed laser source (Ekspla NL202) to excite crystalline solids and nanostructures. Here, we only briefly summarize our experimental studies. A more thorough description can be found elsewhere [15–17]. Our laser delivers optical pulses with a duration of 7 ns, a pulse energy of 2 mJ at a wavelength of 1064 nm at a repetition rate of 1 kHz. To synchronize the arrival of optical and x-ray pulses, a prerequisite to set the pump-probe delay, we feed a bunch marker signal to a pulse and delay generator (Stanford Research DG654). This device generates the necessary trigger signals, namely the pump-probe delay, the external detector gate and the WaveGate timing signal. We control all timing signals through a Tango device server via the beamline control software *spock* [18].

In the first example we demonstrate the timing capabilities of our setup and of the WaveGate pulse picker in particular. Thus, the measurement is performed without a sample so that the direct beam impinges the detector. The blue line in Fig. 5(b) depicts a scan of the relative delay between the detector gate signal and the synchrotron bunch marker. The measurement features individual x-ray pulses with a separation of 192 ns. Here, the WaveGate pulse picker was set in transmission mode, i.e., the x-ray beam is diffracted from the (104) substrate reflex on both the active and analyzer crystal. To set the WaveGate in timing mode, we tilt the active crystal to fulfill the diffraction condition in Eq. (1). The x-ray beam footprint on the WaveGate was 300-400 µm in the diffraction plane. In this geometry the shortest temporal gate possible has a duration of 100 ns. To highlight the SAW propagation through the x-ray footprint, we select five x-ray pulses as shown in the light blue curve in Fig. 5(b). The bunches are modulated in intensity due to the changing overlap of the x-ray beam and the propagating SAW.

This example illustrates that even without single pulse picking the WaveGate enables faster measurement and more efficient use of beamtime. In the direct beam, x-ray pulses impinge the sample with a rate of 5.2 MHz, i.e., much higher than the repetition rate of the laser of 1 kHz. The reduced repetition rate of the time-dependent experiment translates into a reduction of measured intensity of the same ratio, i.e., $I_{MHz}/I_{kHz} = 5,200$. Considering the linear dynamic range of standard hybrid pixel detectors of 80,000 counts/sec/pixel the reduction of the repetition rate poses a serious limitation. Even if the detector records counts only every millisecond in external gating mode all impinging pulses are absorbed. Thus, in external gating mode with repetition rates of 1 kHz, the effective dynamic range is reduced by a factor $80,000/5,200 \approx 15$. In order to not exceed this dynamic range, the x-ray beam must be attenuated by additional absorbers. As a result, the rate mismatch leads to a significant prolongation of the measurement time. A better solution is to match the rate of the measurement and the incident x-ray pulses by installing the WaveGate pulse picker to conserve the full dynamic range of the detector. For our own measurements [17] we used a 10-times shorter integration time due to the WaveGate while maintaining the same number of counts per second on the detector.

Optics EXPRESS

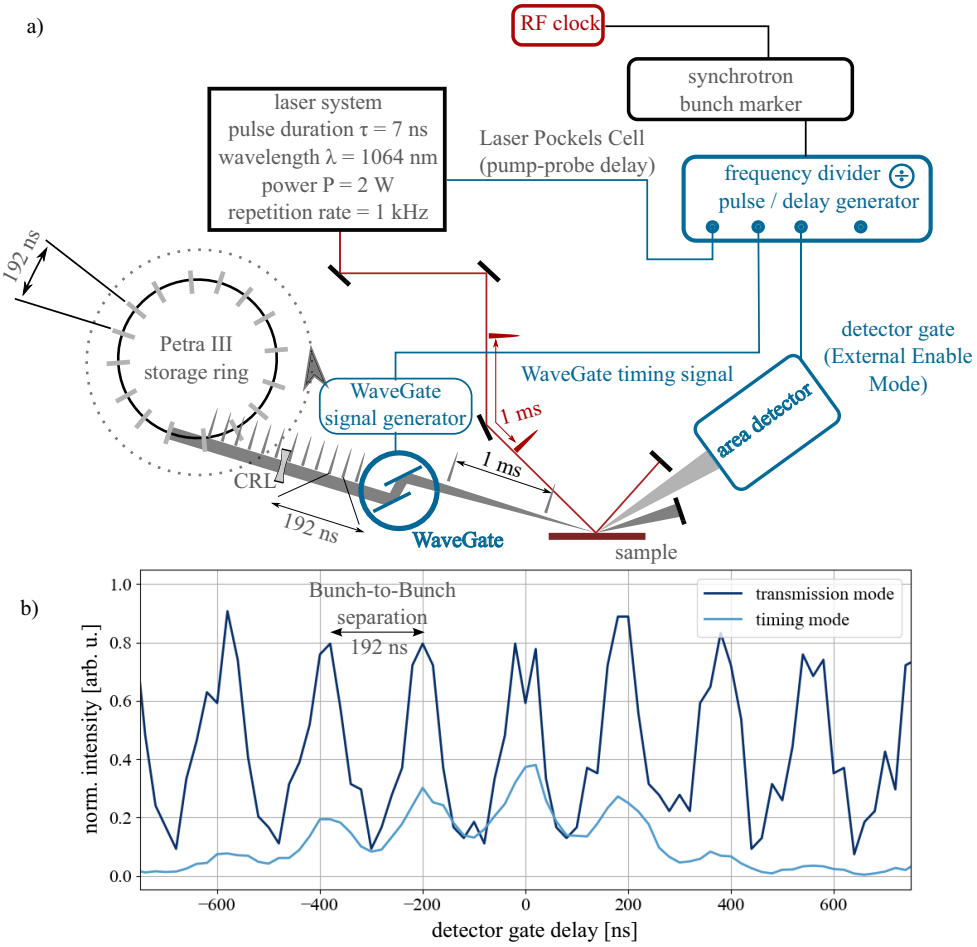

Fig. 5. Optical pump - x-ray probe setup: a) Sketch of the experimental setup. Details are given in the main text or elsewhere [15–17]. The WaveGate pulse picker is used to match the repetition rate of the x-ray probe pulses to the laser pump pulses, thus preserving the full dynamic range of the experiment, as explained in the main text. b) Scan of the external detector gate relative to the synchrotron bunch marker with (light blue) and without (blue) pulse picking by the WaveGate.

Optics EXPRESS

We now discuss a second application of the WaveGate pulse picker, namely the generation of complex pulse sequences for advanced timing schemes [10]. In layman's terms, these concepts consist in probing an excited system with a series of predefined pulse sequences and retrieving the transient state at a certain delay through a linear combination of all measurements. Such concepts are well established for optical [19] applications. However, since the fast temporal modulation of x-ray beams has not been achieved so far, such timing schemes are barely used in the x-ray community.

In Fig. 6(a) and 6(b) we depict two exemplary pulse sequences which were generated with the WaveGate pulse picker. The x-ray beam is modulated on millisecond and microsecond timescales with a constant and variable window size, respectively. Adjacent temporal windows are highlighted in the graph by an alternating gray and white background. For this demonstration we

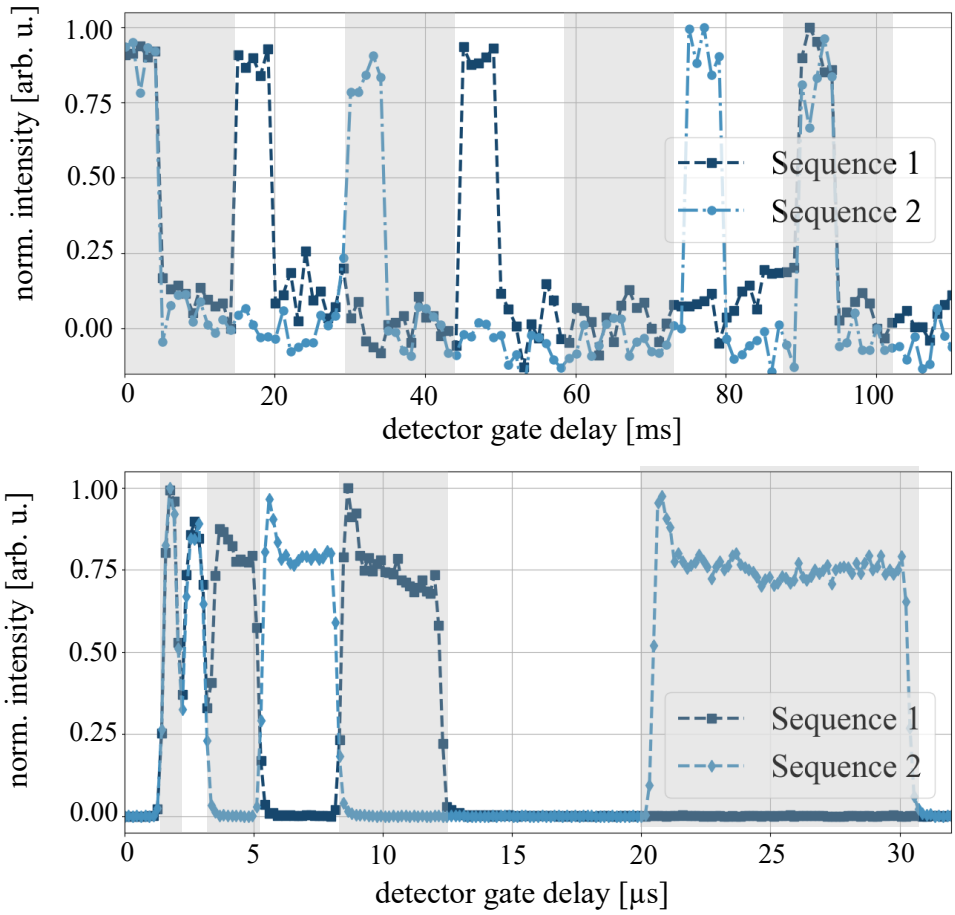

Fig. 6. Pulse sequences for advanced timing schemes: Generation of x-ray probe pulses with a complex time structure. The delay axis is divided into seven windows which are distinguished by the white and grey background. The windows are filled with sequences [1,1,0,1,0,0,1] (sequence 1) and [1,0,1,0,0,1,1] (sequence 2), i.e., the same sequence but shifted by one window to the left. a) The modulation occurs on a ms timescale, the temporal windows have uniform size and the duty cycle within one window is 50%. b) The modulation occurs on a μs timescale, the temporal window size is non-uniform and increases with the delay. The duty cycle of the filling is 100%.

Optics EXPRESS

chose sequences with seven time windows, however, the device does not impose any limits on the length. Sequence 1 is [1,1,0,1,0,0,1] with a duty cycle of 50 % and Sequence 2 is [1,0,1,0,0,1,1] with 100 % duty cycle. In fact, Sequence 2 corresponds to Sequence 1 but translated one time window to the left.

To retrieve information on the dynamics of a system under study, one needs to repeat the measurement with seven different translations of the pulse sequence. The transient state in each temporal window can be retrieved through a linear combination of all measurements. The description of such an experiment is beyond the scope of this article. We will report on a structural dynamics measurement using the Hadamard transform [19], from which these pulse sequences are borrowed, elsewhere.

4. Conclusion

In this article we present a full characterization of the WaveGate pulse picker for hard x-rays at synchrotrons. The device employs propagating SAWs to modulate the diffraction efficiency of an active, piezoelectric substrate. A second analyzer crystal is used to diffract the x-ray beam parallel to its original trajectory towards the experiment. The WaveGate reaches a total efficiency of >30 % of the incident beam, gate opening times as short as 100 ns and an on-off contrast $>10^{-4}$. A main asset of the WaveGate is its enormous flexibility allowing adaptation to various experimental conditions. We also discussed implementation of the WaveGate in a real optical pump - x-ray probe setup and the generation of arbitrary x-ray pulse sequences which enable advanced timing schemes in the hard x-ray regime.

Funding. Deutsche Forschungsgemeinschaft (GA 2558/5-1, GA 2558/7-1, GA 2558/9-1).

Acknowledgment. We acknowledge DESY (Hamburg, Germany), a member of the Helmholtz Association HGF, for the provision of experimental facilities. Parts of this research were carried out at Petra III and we would like to thank Dmitry Novikov and Azat Khadiev for assistance in using Beamline P23 and David von Stetten and Michael Agthe for assistance in using P14. Beamtime was allocated for proposal(s) I-20221397, I-20220569, I-20211492 and MX839. We acknowledge the European Synchrotron Radiation Facility (ESRF) for provision of synchrotron radiation facilities and we would like to thank Edoardo Zatterin for assistance and support in using ID01.

Disclosures. The authors declare no conflicts of interest.

Data availability. Data underlying the results presented in this paper are not publicly available at this time but may be obtained from the authors upon reasonable request.

References

1. C. G. Schroer, H.-C. Wille, O. H. Seeck, *et al.*, "The synchrotron radiation source petra iii and its future ultra-low-emittance upgrade petra iv," Eur. Phys. J. Plus **137**(12), 1312 (2022).
2. M. Bieler, I. Agapov, Y.-C. Chae, *et al.*, "Petra III Operation and Studies 2018," in: *Proc. 10th International Particle Accelerator Conference (IPAC'19), Melbourne, Australia, 19-24 May 2019, no. 10 in International Particle Accelerator Conference, JACoW Publishing, Geneva, Switzerland*, 2019, pp. 1419–1421, doi:doi:10.18429/JACoW-IPAC2019-TUPGW015. URL http://jacow.org/ipac2019/papers/tupgw015.pdf
3. "Esrf operation modes," (2023). https://www.esrf.fr/Accelerators/Operation/Modes
4. "Aps operation modes," (2023). https://ops.aps.anl.gov/SRparameters/node5.html
5. P. Gaal, D. Schick, M. Herzog, *et al.*, "Time-domain sampling of x-ray pulses using an ultrafast sample response," Appl. Phys. Lett. **101**(24), 243106 (2012).
6. H. Enquist, H. Navirian, R. Nüske, *et al.*, "Subpicosecond hard x-ray streak camera using single-photon counting," Opt. Lett. **35**(19), 3219–3221 (2010).
7. M. Sander, A. Koc, C. T. Kwamen, *et al.*, "Characterization of an ultrafast bragg-switch for shortening hard x-ray pulses," J. Appl. Phys. **120**(19), 193101 (2016).
8. M. Sander, R. Bauer, V. Kabanova, *et al.*, "Demonstration of a picosecond Bragg switch for hard X-rays in a synchrotron-based pump–probe experiment," J. Synchrotron Radiat. **26**(4), 1253–1259 (2019).
9. S. Vadilonga, I. Zizak, D. Roshchupkin, *et al.*, "Pulse picker for synchrotron radiation driven by a surface acoustic wave," Opt. Lett. **42**(10), 1915–1918 (2017).
10. B. A. Yorke, G. S. Beddard, R. L. Owen, *et al.*, "Time-resolved crystallography using the hadamard transform," Nat. Methods **11**(11), 1131–1134 (2014).
11. P. Hess, "Surface Acoustic Waves in Materials Science," Phys. Today **55**(3), 42–47 (2002).
12. https://x-server.gmca.aps.anl.gov, accessed: 20120-06-11.

Optics EXPRESS

13. M. Rössle, W. Leitenberger, M. Reinhardt, *et al.*, "The time-resolved hard X-ray diffraction endstation KMC-3 XPP at BESSYII," J. Synchrotron Radiat. **28**(3), 948–960 (2021).
14. S. Vadilonga, I. Zizak, D. Roshchupkin, *et al.*, "Piezo-modulated active grating for selecting x-ray pulses separated by one nanosecond," Opt. Express **29**(22), 34962–34976 (2021).
15. D. Schmidt, R. Bauer, S. Chung, *et al.*, "A new concept for temporal gating of synchrotron X-ray pulses," J. Synchrotron Radiat. **28**(2), 375–382 (2021).
16. D. S. K. N. P. G. Stefan Schwabe, K. Lünser, and S. Fähler, "What is the speed limit of martensitic transformations?" Sci. Technol. Adv. Mater. **23**(1), 633–641 (2022). pMID: 36212679
17. P. Gaal, D. Schmidt, M. Khosla, *et al.*, "Self-stabilization of the equilibrium state in ferroelectric thin films," Appl. Surf. Sci. **613**, 155891 (2023).
18. T. Coutinho, G. Cuní, D. Fernandez-Carreiras, *et al.*, Sardana, the software for building scadas in scientific environments (11 2023).
19. E. D. Nelson and M. L. Fredman, "Hadamard spectroscopy," J. Opt. Soc. Am. **60**(12), 1664–1669 (1970).